NRIAG JOURNAL OF ASTRONOMY AND GEOPHYSICS
2021, VOL. 10, NO. 1, 76–92
https://doi.org/10.1080/20909977.2021.1880043

Source structures at Pre-Miocene level as deduced by gravity stripping

Ahmad Azab and Shokry Soliman

Exploration Department, Egyptian Petroleum Research Institute, Cairo, Egypt

ABSTRACT

The lowermost portion of the sedimentary section in Gulf of Suez basin is mostly of low resolution and hardly interpret. This may be attributed to the bad seismic reflection that stops at a certain limit and fails to reach the deep settings, or due to non-coverage of boreholes. Herein, the gravity data was reinterpreted utilizing the stripping technique as an alternative tool to overcome the seismic failure. The process simply consists in calculating the gravity effects of the shallow rock-units and removing them from the Bouguer map, then in analyzing the remaining gravity. The ordinary seismic analysis was performed to control the geometry of the Miocene–Post Miocene formations, and density was driven from boreholes. Further analyses were done on the stripped map to obtain details about the deep sources. Generally, the study suggests a complex structure at Pre-Miocene level more than that of Miocene. It delineates two main troughs; Miocene basin to the east and Pre-Miocene basin (involves three sub-basins) to the west, separated by a structural ridge, all are northwesterly oriented. The basement is very disturbed by cross-faults, with no evidence support presence of igneous intrusions along. Two different forces (NW-SE compression and NE-SW tension) affected the region.

ARTICLE HISTORY
Received 30 July 2020
Revised 12 January 2021
Accepted 18 January 2021

KEYWORDS
Gulf of Suez; applied geophysics; gravity stripping; Ras Shokeir; Ras Gharib

1. Introduction

The Gulf of Suez (GOS) area (Figure 1(a)) is one of the most prolific and prospective oil provinces in Egypt. The exploration potential of the southern portion of the GOS bears a prospective future for finding additional hydrocarbon reserves, primarily in the Miocene reservoirs. Also, accumulation in the Pre-Miocene clastic sequence has an input to the cumulative oil potential. The development of sedimentary basins during Upper Cretaceous-Oligocene times may have an impact on the distribution of the source/reservoir rocks. The majority of the oil fields incorporate multiple productive reservoirs of Miocene and Pre-Miocene. Generally, the sedimentary section in the GOS are classified into; 1) pre-rift which includes (Paleozoic–Early Cretaceous Nubian sandstones A, B, C, and D, Upper-Cretaceous Nezzazat Fm. (sandstones), Eocene Thebes Fm. (fractured limestone)), and 2) syn-rift which includes (the sandstones and carbonates of Nukhul, Rudeis, Kareem, and Belayim Fms., and the sandstones within the South Gharib and Zeit Fms). The Miocene evaporites are the ultimate seals/traps of hydrocarbons in the syn-rift stratigraphic units, whereas the shale and dense limestones are the primary seals of the pre-rift interval (Said 1990; Alsharhan 2003).

Most of oil fields in the GOS area terminate from the east and west by NW-SE major faults (Clysmic trend), and from the south and north by NE-SW cross-gulf trending faults (Moustafa 1976). At low depths, mapping of these cross-faults and associated structures could be obtained from the seismic interpretation and/or available wells data. But, at deep depths, this become more difficult or nearly impossible due to the low resolution of seismic survey or the none-coverage of boreholes. The blind zone on seismic sections, where seismic reflectivity is not good, is mostly attributed to the presence of noising effects due to salt structures. Lamination of the evaporite rocks often conceals the deep signals, and causes bad seismic reflection at top of Pre-evaporite strata. Gravitationally, the thickness changes and density variations of the Miocene evporite create anomalies like those arise from the Pre-Miocene (PM) uplifts, which may conceal or obscure the deep source structures. This makes it difficult to delineate the deep structural elements, especially cross-fault structures which are of upmost importance in delineating the location and size of the oil fields and control migration of the hydrocarbons and sedimentation (Meshref 1990; Azab et al. 2018).

The gravity anomalies in the region are considered to be the sum of the gravity effects due to the structural and lithologic variations of four main depositional packages; the Post-Miocene, Middle-Miocene, Lower-Miocene, and Pre-Miocene, as well as the basement rocks. In fact, the traditional methods of analysis is inadequate to right-interpret the deep structures due to contaminations which result from shallow features. Therefore, the gravity stripping approach (Bible and John 1961; Hammer

CONTACT Ahmad Azab a.abdelhayazab@yahoo.com Exploration Department, Egyptian Petroleum Research Institute, Cairo, Egypt

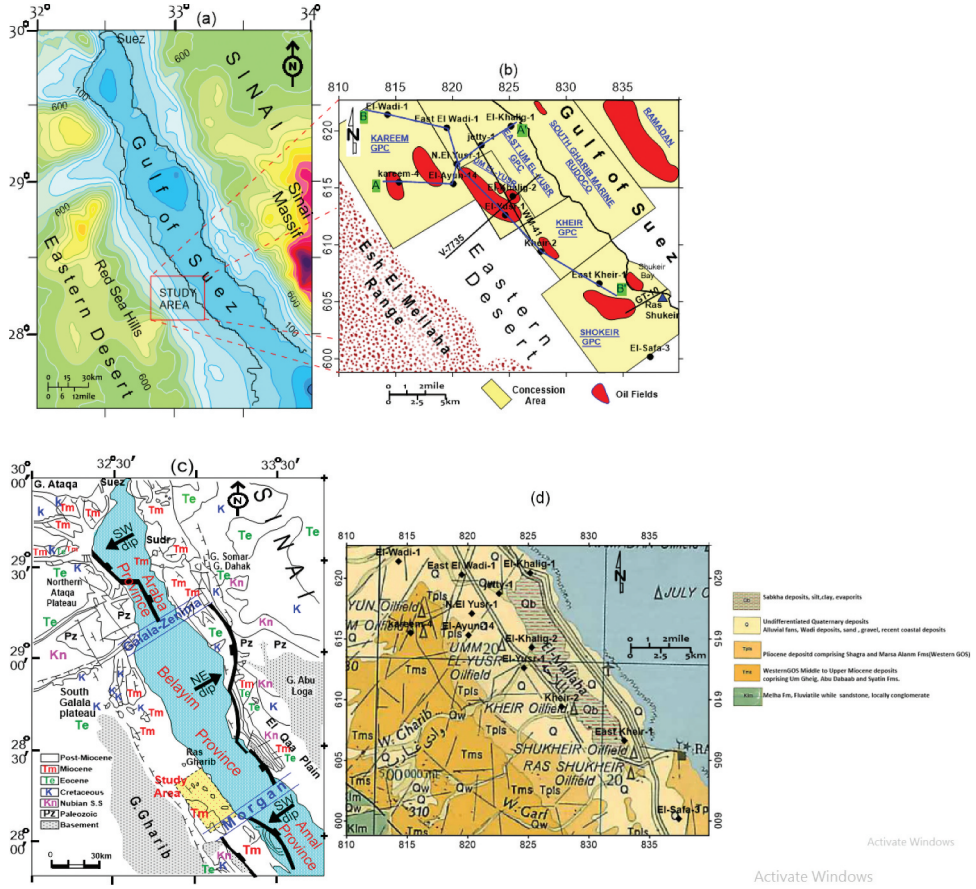

Figure 1. Location map of the study area showing (a) topography of the Gulf of Suez, and surrounding area (from GTOPO30 data set, after Gesch *et al.* 1999),(b) distribution of the different oil field concessions, drilled wells, locations of geologic cross section, drilled wells, seismic lines and modelled profiles. (c) Tectonic provinces of the Gulf of Suez (modified after Mostafa1992), (d) surface geological map of the study area.

1963) was used to eliminate the bad gravity effects of shallow features and to obtain a new gravity map for the deeper constituents.

Many authors used the gravity stripping technique for identification of the deeper sources/structures of gravity anomalies (e.g. Abu El-Ata and Helal 1985, 1986; Bielik 1988; Rybakov et al. 1998; Alasonati et al. 2008; Vajda et al. 2008; Simeoni and Brueckl 2009; Tenzer et al. 2009; Krajňák et al. 2012; Bielik et al. 2013). The stripping process is based on isolation of the gravity effects of the shallow part (Miocene and Post-Miocene), which seismically identified, away from that of an unknown portion (Pre-Miocene). This was done through several consecutive steps and calculations that require a structural control through seismic lines interpretation to define the geometry, and a lithologic control through wells data to determine the formation density. The gravity effect for each rock-units above the datum (top Pre-Miocene) was computed and subtracted from the Bouguer data to compile a new gravity map (stripped map) on top of the Pre-Miocene. Further treatment and analysis were carried out on the stripped off map to explore the deep settings in which seismic is unable to shed light on. The qualitative and quantitative interpretation were discussed in terms of geology and tectonics of the GOS. The steps of calculations were performed in a grid-like forms, having the same grid-nodes of the coordinates (X = 18; Y = 36).

The objective of this study is to delineate the characterisation of the prevailing subsurface structures and their tectonic position in the lowermost portion of the sedimentary section in the Gulf of Suez basin. The main task is to obtain a stripped gravity map on top of Pre-Miocene sequence, which is suitable for interpreting the poorly understood deep structure-tectonic settings. Certain emphasis was put on the basement uplifts, detection of the cross-faults and delineating the Pre-Miocene basins, which may provide favourable conditions for oil accumulations.

2. Dataset

The Bouguer anomaly map, with scale of 1:100,000, contour interval of 2 mGal has been compiled by the General Petroleum Company (GPC) in 1986, and was digitized and used to display the gravitational field in/around the study area. The gravity survey was performed by Anglo Egyptian Oilfield Ltd. using the

Askania torsion balance with a resolution of 0.1 mGal to produce a map with contour interval of 0.5–1 mGal. The dataset was compiled, classified and ranked according to the sensitivity of the instruments and density of the measurements. The seismic studies carried out were based on eighteen seismic lines, oriented in the NW and NE directions. They were acquired by Geophysical Service International Company at 1981 under auspices of the Egyptian General Petroleum Corporation. These lines passed through several wells (Table 1), which are used as a start points for identifying and controlling the reflectors on the seismic sections.

3. Geologic settings

The GOS looks as a great elongated depression separated between two massifs; Sinai to the east and African-Nubian to the west, where the average distance between these two shield masses is ~85 km. The offshore gulf extends ~320 km long and an average width of water of ~30 km. The study area (Figure 1(b)) lies in the southern portion, along the western coast of the GOS. It occupies the onshore part that limited by Ras Gharib in the north to Ras Shokeir in the south, and confined between Red Sea Hills to the west and the GOS basin to the east. The area considered as a part of Clysmic gulf (old GOS), and contains the same structural characteristics of the Arabo-Nubian rocks.

The structural-tectonic framework of the GOS was studied by many authors (e.g., Moustafa 1976, 1993; Garfunkel and Bartov 1977; Montenat et al. 1998; Sharp et al. 2000; Bosworth et al. 2014, 2016). They concluded that the GOS area consists mainly of three tectonic provinces (Figure 1(c)) namely Galala, Belayim, and Amal, as arranged from north to south. They were separated from each other by two accommodation zones; Galala-Zenima to the north and Morgan to the south (Moustafa 1976) or transfer zones (Patton et al. 1994; Morley et al. 1995). The northern and southern tectonic provinces are characterised by a regional SW dip regime, while the middle one is sloping generally in the NE direction (Bayoumi 1983; Meshref 1990). Along both sides of the GOS there is a major marginal fault zone marked by lines of high escarpments bordering the depression (Gupta et al. 1999). Westward, the basement exposure (Esh El-Mellaha Range) is characterised by dense fractures, where the major Clysmic faults were cut obliquely by transfer faults parallel to the Gulf of Aqaba. The offshore basement structure to the east is expected to be a prolongation of the exposed onshore one (Abu El-Ata and Helal 1985).

Previous stratigraphic studies in the GOS area (e.g. Schlumberger 1984; McClay et al. 1998; Bosworth and McClay 2001. Sharp et al. 2001; Young et al. 2002; Jackson 2008; Khalil and McClay 2008; Hewaidy et al. 2016; Pietrantonio et al. 2016; Rohais et al. 2016; Bosworth and Durocher 2017; Segev et al. 2017; Temraz and Dypvik 2018) indicated that the stratigraphic section of the GOS basin can be divided into three major units of different thicknesses, depositional environments, areal distributions, and hydrocarbon potentialities. The inside of the GOS consists of Miocene and Post-Miocene rocks while outside the depression, the high relief ridges are built of basement rocks in the southern portion, followed to the north by Palaeozoic-Cenozoic sediments (Figure 1(c)). The Pre-Miocene section is essentially formed of a thick sequence of argillaceous sandstone of Nubia facies of Carboniferous-Cretaceous age, unconformably overly the Precambrian basement rocks. The late Cretaceous-Eocene time is characterised by marine sandstone, shale, limestone, and chalk. The Miocene deposits which consist of two groups, Lower-Miocene Gharandal group at the base, and Middle-Miocene Ras Malaab at the top. The predominantly clastics group comprises the Nukhul, Rudeis, and Kareem formations, which are mainly shales with subordinate carbonate reefs and anhydrite beds. The predominantly evaporitic group consists of salts-anhydrites interbedded with shales and occasionally with sands and limestone streaks. The Upper-Miocene is nearly absent in this basinal area, because of a major unconformity between the Miocene and Post-Miocene deposits. The Post-Miocene section (Tor group) is

Table 1. Parameters of available wells drilled in the study area.

Name	Easting	Northing	T.D	Fms	STATUS
El-Wadi-1	814.28258	621.40141	1834.4	Palaeozoic	P & A WITH OIL SHOWS IN THE MIOCENE
East El Wadi-1	819.50867	620.30642	2162	Miocene Rudeis	P & A
El-Khalig-1	825.12973	620.45033	3625	Basment	P & A
jetty-1	822.56425	618.7424	3140.39	Turonian	P & A
El-Ayun-1	820.058058	615.33146	1328.7	U.Cret.	OIL PRODUCER MIOCENE DISCOVERY
kareem-4	815.28447	615.49471	854	Cret.	OIL PRODUCER MIOCENE & EOCENE DISCOVERY
El-Khalig-2	825.26695	614.29381	2126	L.Eocene	P & A
El-Yusr-1	824.65369	612.61975	1588	Eocene	OIL PRODUCER MIOCENE DISCOVERY
Kheir-2	827.7688	609.4048	1901	Miocene	P & A WITH OIL SHOWS IN THE MIOCENE
East Kheir-1	832.922922	606.61995	2037	Eocene	P & A
El-Safa-3	837.39687	600.182	2032	L.Miocene	P & A
N.El Yusr-1	820.35	617.1128582	150.2	Eocene	P & A

essentially composed of sands, and clays and occasional anhydrite, and limestone near the bottom (Schlumberger 1984). Figure 1(d) presents the surface geology of the study area (EGPC, 1986).

4. Methodology

The stripping process requires a precise determination of the changes in thickness and density of each layer in the sequence to right calculate their gravity effects. The thickness/depth of the sedimentary layer was obtained through doing a conventional seismic data interpretation, which gives details on the geometry of the Tertiary-Quaternary formations. The seismic analysis carried out depends on a set of seismic lines (Figure 2) cutting the area in two different directions (NW and NE), tied with VSP of the drilled wells. Figure 3 shows examples of the relationship and velocity measurements of various strata penetrated by drilled wells. The ordinary steps include distinguishing of stratigraphic boundaries, correlation of the real reflections, and fault detection direction on the recorded sections. The interpretation ultimately led to construct a number of isochronous reflection (time) maps on tops of the Miocene strata, which were converted into depth maps using the average velocity. At last, a set of isopach maps for the major stratigraphic units were established to be used in the stripping process, as a geometric control. The density contrast for every rock unit was determined from its actual density contrasted to the basement density.

As soon as the new gravity map on top of Pre-Miocene rocks had been obtained, it was subjected to further processing techniques to obtain details about deep sources. The first-order vertical derivative (FVD) filter was applied for eliminating the deep crustal effect which is corresponding to the Moho gravity effect. The filter is very useful in removing the regional gravity trend, and in enhancing some local anomalies which do not exist before. The maximum horizontal gradient map was prepared and overlapped with the curvature map to demarcate locations of the cross-faults on basement surface. The Euler deconvolution solutions were computed and interpreted in terms of linear and curved fashion which separate between the different gravity zones. The SPI method was also estimated to detect the locations and approximate depths to the deep gravity sources. Statistical trend analysis of the lineaments was applied on tops of the stripped map to follow up the deep structural trends. The stress-strain

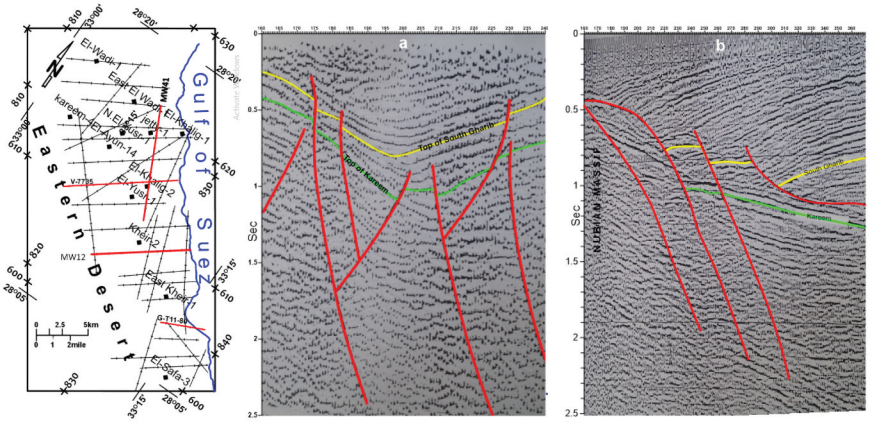

Figure 2. Shot point location map with two examples of the interpreted seismic lines (a) GT-11-800 and (b) V-7735.

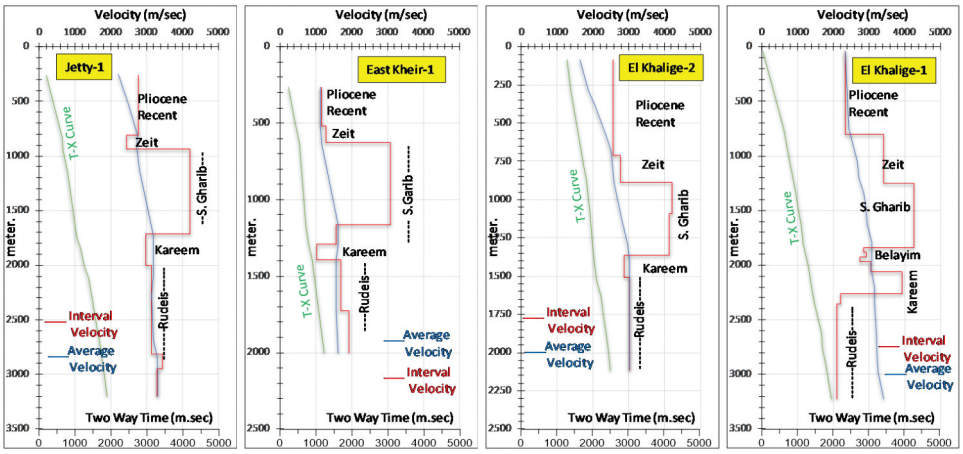

Figure 3. Examples of time–depth curve measurements and velocity determinations of different drilled well.

diagram (tectonic model) was designed to define the main tectonic forces affecting the area; their types, trends, and time of durations. The analysis of these tectonic stresses in relation to plates deformation has been done to explain the structural complexity in the area and giving an idea about its geologic history. A comparative study of the gravity anomalies before and after the stripping was carried out through applying the 2½D modelling, to confirm the shallower features and deduce the deep source structures. Also, 2D combined gravity-seismic models were constructed along with two different directions to more control shallower structure and to explain the deeper configurations. Figure 4 shows a flowchart used for the study. It represents a workflow or a diagrammatic representation of the work, a step by step approach to interpret the data.

5. Geometrical considerations

The seismic interpretation led ultimately to establishing a set of thickness maps to control the geometry of different lithologic units. Isopach map of the Pliocene-recent sediments (Figure 5(a)) exhibits a large thickness (~900 m) in the eastern part, which decreases westward to reach ~50 m as a minimum. The isopach map of the Middle-Miocene sediments (Figure 5(b)) show a great section of the evaporites which was excessively deposited along the shoulder of the gulf (>2000 m), while a lesser section (<200 m) was found

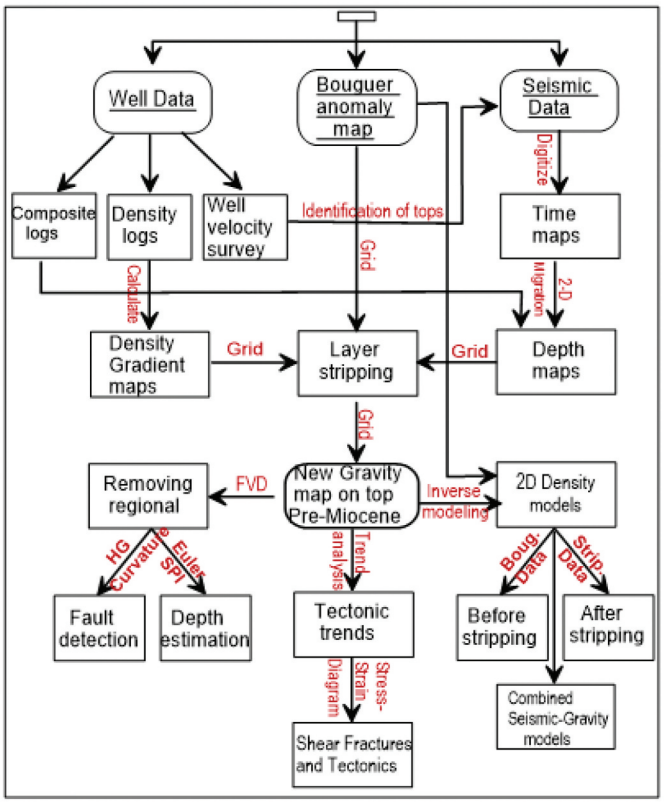

Figure 4. Work flowchart.

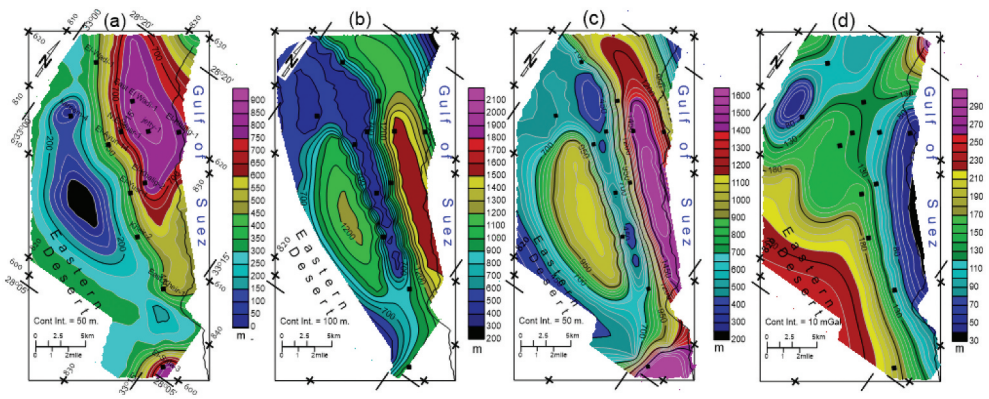

Figure 5. Seismic isopach maps of (a) Post-Miocene, (b) Middle-Miocene, (c) Lower-Miocene and (d) Eocene-Paleocene.

alongside the Red Sea Hills. Isopach map of the Lower-Miocene sediments (Figure 5(c)) shows that the largest thickness of Rudeis sands was deposited in the eastern basin (~1600 m), while the smallest thickness (~200 m) was recorded in the western basin. Figure 5(d) shows a different pattern of distribution, where a large thickness of the Palaeocene-Eocene sediments were accumulated in the west (~300 m) and decreases towards the east (30 m). Generally, the isopach maps show a large variation in thickness from east to west, where the Miocene–Post-Miocene basin was essentially deposited alongside the rift-soulder, while the Pre-Miocene basin was formed alongside the Nubian Massif. The isopach maps are characterised by a conspicuous thinning in the centre, which is correlated with a NW-SE longitudinal ridge.

6. Heterogeneity considerations

Another important element that is very effective in calculating the gravity effects of the different rock-units is the density. The measurements obtained from different boreholes indicate that the density is not linearly correlated with depth, because of the lithology varies vertically and horizontally. To overcome density heterogeneity, the actual density derived from the wells data was averaged for each lithostratigraphic unit and used to construct a density-gradient map. The most reliable density of the sedimentary formations was obtained from gamma-gamma logging, or based on formation density compensated log (FDC) of ten wells scattered in the area. The density logs of the surface layer (Pliocene-Recent) are mostly missed and considered to be constant (~2200 kg/m^3). The density gradient map of the Miocene evaporites (Figure 6(a)) is characterized by a wide range (2000–3000 kg/m^3), with a noticeable increase from the southeast to northwest. The low density relates with excessive salt rocks (halite) intercalated with sandstone deposits while the high density is expected to be associated with anhydrite accumulations and/or dense shales. The density gradient map of the Lower-Miocene formations (Figure 6(b)) is characterised by a narrow range (2250–2550 kg/m^3) which relates to the Rudeis sands. The map exhibits a low-density zone elongate in the NW direction, overlay a structural high separation between the eastern and western basins. The density of the basement rocks (2600–2700 kg/m^3) was assigned from the laboratory measurements of core samples at Safa-3 well in the southern area.

7. Qualitative interpretation of Bouguer anomaly map

The Bouguer anomaly map (Figure 7) is generally characterised by a low-gravity field everywhere, which may suggest a thick sedimentary cover and/or low-density source rocks. The map is dominated by negative gravity values range from −30 to −50 mGals, which generally increase towards the south. It comprises a set of high and low anomalous features that are running nearly parallel or perpendicular to the GOS province. Northward, the gravity field exhibits two broad gravity lows to the east and west, which are separated from each other by a high anomalous feature extend in the N-S direction. These two

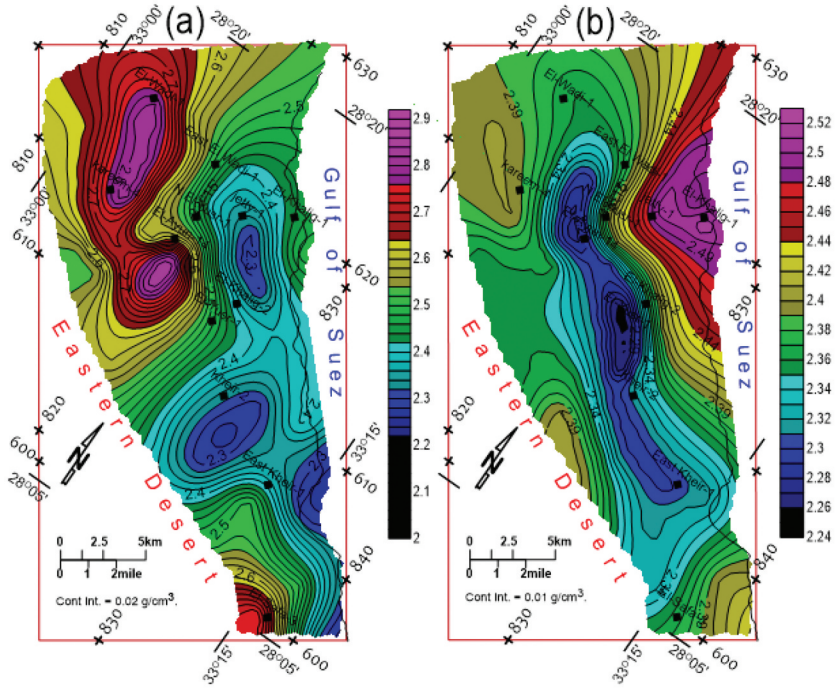

Figure 6. Density-gradient maps of (a) Middle-Miocene and (b) Lower-Miocene.

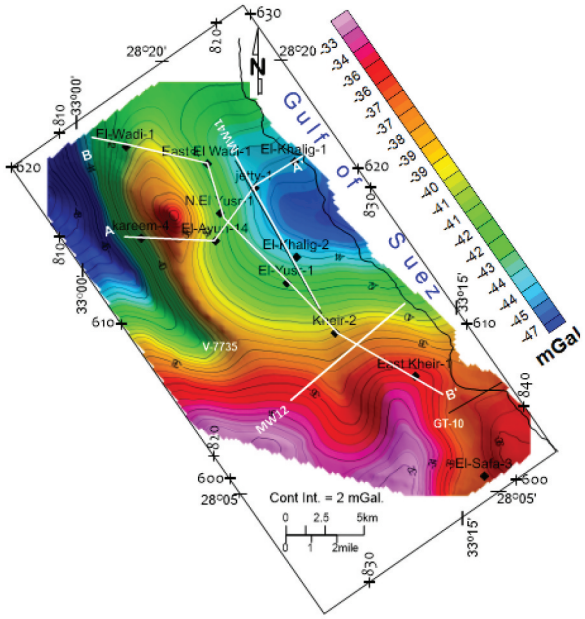

Figure 7. Bouguer gravity map of the study area, showing locations of the modelled profiles, cross-section profile and seismic profiles.

gravity minima are correlated with two basinal areas alongside the rift-shoulder and Nubian Massif, while the gravity maximum corresponds to a basement ridge. The steep gravity gradients and linear structures mostly mark locations of major faults between basement blocks. Southward, the gravity values increase rapidly towards the southwest corner associated with the shallow basement rocks of Esh Elmellaha Range. The undulation in the gravity contours west of Shokeir may reflect subsurface structural manifestations.

8. Gravity effects

Herein, the gravity effects of the Miocene and Post-Miocene formations were estimated through applying layer stripping on the Bouguer data based on the seismic results and wells controls. The calculation for each rock unit was done in a regularised grid form, and sequentially subtracted from the Bouguer-grid, producing a new gravity map (stripped map) of Pre-Miocene sequence (top Thebeis Fm), which is more reliable to interpret the deep constituents after eliminating the shallower contaminations.

The general equation used for stripping of the different rock unit in the sedimentary sequence is

$$\Delta g_e = 2\pi G \Delta\rho_e \, H_e \qquad (1)$$

where:

Δg_e is the gravity effect of certain unit in (mGal), G is the international gravitational constant (6.67 x 10^{-8} $cm^3/g.s^2$), $\Delta\rho_e$ is the density contrast between the formation density and the datum density in g/cm^3, H_e is the thickness of the rock unit in cm.

The geometry/thickness of the different rock units has been seismically controlled by the seismic isopachs. The formation density was driven from the wells data, and used to construct a set of density-gradient maps. According to Otsuka and Ogawa (1977), the gravity effect above the datum (top Pre-Miocene) given by

$$\Delta g_{strip} = \Delta g_{Boug} - \left(\Delta g_{Pz} + \Delta g_{MM} + \Delta g_{LM}\right) \qquad (2)$$

where:

Δg_{strip} is the gravity effect after stripping; Δg_{Boug} is the gravity effect before stripping; Δg_{Pz} is the gravity effect of Post-Zeit; Δg_{MM} is the gravity effect of Middle-Miocene; Δg_{LM} is the gravity effect of Lower-Miocene.

$$\Delta g_M = 2\pi G\begin{pmatrix}(\rho_Z - \rho_b)H_Z + (\rho_{SG} - \rho_b)H_{SG} + (\rho_B - \rho_b)H_B + \\ (\rho_K - \rho_b)H_K + (\rho_R - \rho_b)H_R + (\rho_N - \rho_b)H_N\end{pmatrix} \qquad (3)$$

Pz = Post-Zeit (Post-Miocene), MM = Middle-Miocene, LM = Lower-Miocene Z = Zeit Fm., SG = South Gharib Fm., B = Belayim Fm., K = Kareem Fm., R = Rudeis Fm., N = Nukhul Fm., b = basement.

Equation (3) was calculated for every rock unit and the outputs were contoured using Surfer 16 Golden Software.

The post-Miocene sediments is characterised by a negative gravity effect (Figure 8(a)) which ranges between −18 mGal and −0.5 mGal, which could be attributed to the low density of the surface layer. The Middle-Miocene section shows a high gravity effect

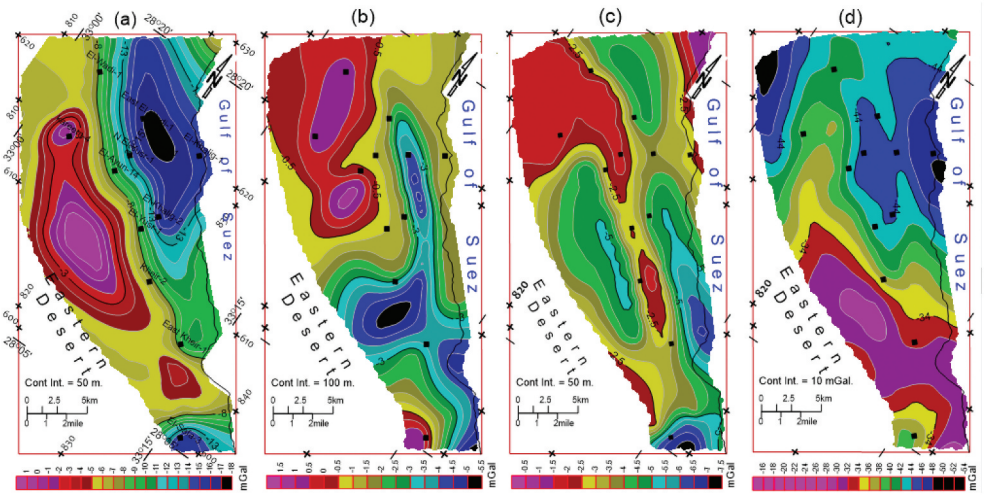

Figure 8. Gravity effect of the (a) Pliocene-Recent, (b) Middle-Miocene, (c) Lower-Miocene, and (d) stripped gravity effect on top of Pre-Miocene.

(Figure 8(b)) and varies from 2 mGal (westward) to −5.5 mGal (eastward) which could be due to the dense evaporite rocks. The Lower-Miocene deposits exhibit a negative gravity effect (Figure 8(c)) ranges from −0.5 mGal to −7.5 mGal, which closely relates to low-density of the Rudeis Fm. The gravity map of Pre-Miocene section (Figure 8(d)) was obtained through subtracting Figure 8(a), Figure 8(b) and Figure 8(c) from the Bouguer anomaly map (Figure 7). The map displays the largest gravity effect (from −15 to −55 mGal), which indicates that the most gravity anomalies are of deep-seated origin.

9. Gravity filtering

The vertical derivatives methods of the observed gravity field are widely used in the interpretation of gravity data. The importance of the first/second-order vertical derivative comes from the fact that it leads to remove the regional components of higher orders. The filter emphasise the shallow anomalies, enhances the minor features, gives better resolution of some anomalies which do not appear clearly in the original gravity map, and aids in defining the edges of source bodies. Herein, the simple theoretical formula after Henderson and Zeitz (1949) was applied in space domain on the stripped anomaly map (Figure 8(d)), using Surfer 16 Golden Software (in-house filter). The first-order vertical derivative map (Figure 9(a)) shows alternated high and low gravity zones, running parallel to the GOS trend in the NW direction. The correlation with the drilling information indicates that the gravity minima (labelled 1, 2, 3 and 4) are associated with sedimentary basins while the gravity highs are closely

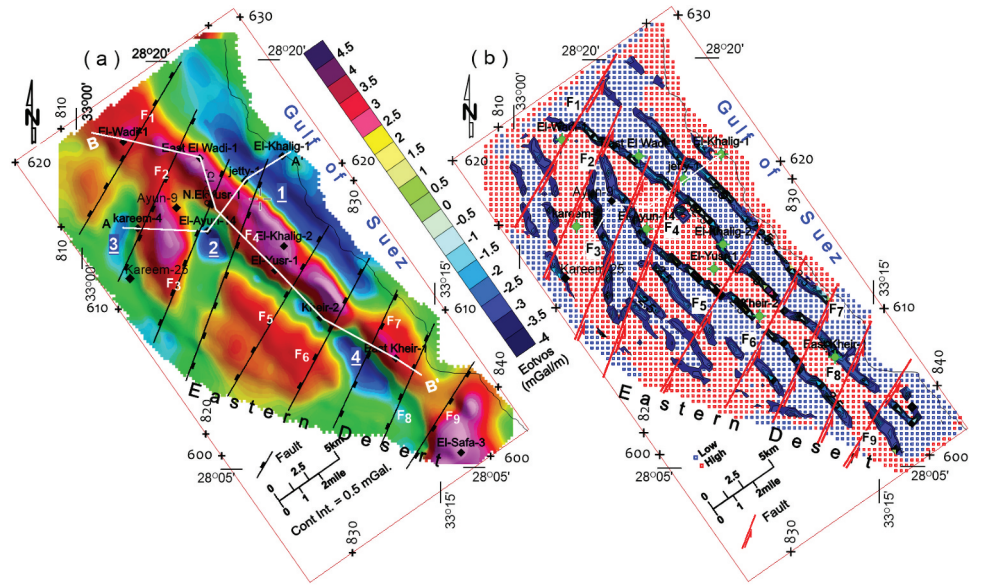

Figure 9. Gravity filtering of the (a) first-order vertical derivative map of the stripped gravity anomalies on top of Pre-Miocene,and (b) maximum curvature map and horizontal gradient maxima of the stripped gravity anomalies on top of Pre-Miocene rocks.

linked with Pre-Miocene uplifts. The steep gradients between anomalies mark locations of the boundary faults between basement blocks.

The horizontal gradient (Nabighian 1972) and the maximum curvature (Roberts 2001) filters were applied on the stripped gravity data using Oasis Montage Package V.8.3. (2014), to reveal more the structural lineaments at Pre-Miocene level. The overlapped curvature and horizontal gradient map (Figure 9(b)) show three gravity lows (blue) alternated with three high (red) gravity zones, all are running parallel to the main GOS trend. The linear features (black) point to locations of major NW-trending faults bordering the blocks from the east and west, which divided the basement surface into horsts and grabens. The discontinuity of these linear structures is attributed to right-lateral displacements in the NE direction, parallel to the Aqaba trend. The longitudinal faults (Clysmic trend) are not long continuous features, but were obliquely cut and offset by a number of cross-gulf faults (Aqaba trend), labelled (F1-F9). Generally, the structural elements deduced from Figure 9(b) agree with those that exist in Figure 9(a).

The deep fault trends on the basement surface were confirmed by applying the Euler deconvolution method (Reid et al. 1990), which serves to determine source positions, edge locations, and depths of inhomogeneity. The method was applied on the FVD map (Figure 9(a)) with a structural index = 0 and window size = 10, using Euler3D software included in Oasis Montage Package, (2014). The results were plotted in (x, y) positions using coloured symbols (circles) that are proportional to the depth (z). The Euler solutions (Figure 10(a)) have clustered along steep gradient zones between anomalies. They indicate that the subsurface structure is dominated by cross-faults that belong to the NW (Clysmic) trend and the NE (Aqaba) trend. More or less, these linear structures are consistent with those deduced from HG maxima (Figure 9(b)).

Source Parameter Imaging (SPI) function was applied to determine the depth to causative sources, source geometries and density contrast (Nabighian et al. 2005). The depths to the gravity sources were determined without assumptions about the thickness of their sources. The principle, theory, formulation, and application of the SPI were discussed by many authors (e.g. Thompson 1982; Roest et al. 1992; Nabighian et al. 2005; Reeves 2005). Practically, the source parameter imaging was applied using SPI software included in Oasis Montage Package (2014). The calculations were carried out on a gridded-data of the new gravity map on top of Pre-Miocene (Figure 8(d)). The depth has estimated through a number of pre-processed grids dx, dy, and dz which were calculated and serve as inputs for SPI calculations. The calculated depths to their sources were displayed as an image which makes the interpretation easier. Generally, the outputs obtained from the application of the SPI method (Figure 10(b)) show great changes in depth to the basement which ranges between 0.3 and 3.5 km. The map exhibits five gravity lows labelled 1,2,3,4 and 5, delineate five basinal areas correspond to "W. Kareem, S.El-Yusr, and W.El-Kheir" basins to the west and "El-Khaligue depression" to the east. These fill-sediment basins were separated from each other by a structural ridge extends from Ayun–Yusr–Kheir, all of which are westerly oriented parallel to the GOS trend. Such a Pre-Miocene uplift is considered as a focal point in trapping oil from the neighbouring low areas.

The trend analysis (Affleck 1963) is a method by which the tectonics of the area can be determined, where the tectonic history of the rocks can be recorded from the magnitudes and patterns of their gravity anomalies. The cross elements were traced on top of

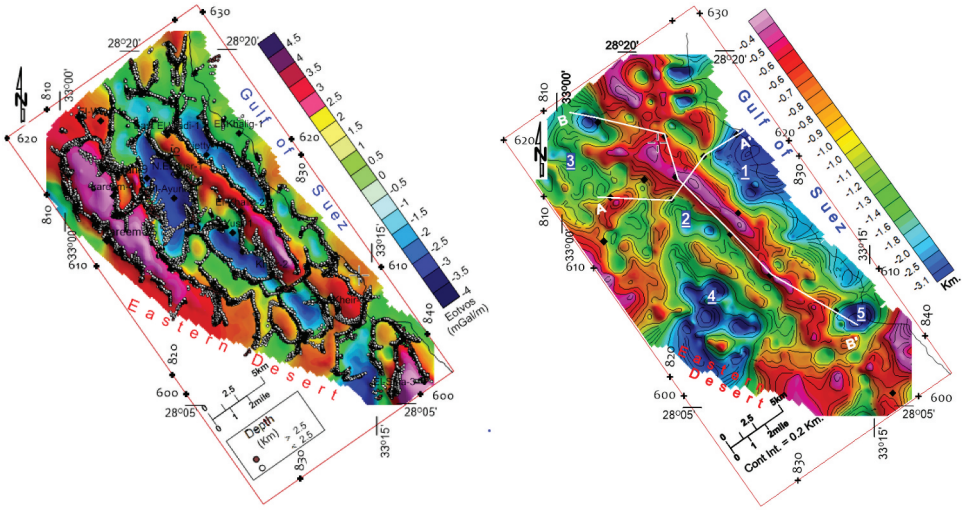

Figure 10. (a) Euler Deconvolution applied on the FVD of the stripped map (b) basement relief map of the study area as deduced from the stripped map on top of Pre-Miocene by using source parameters imaging (SPI).

Table 2. Parameters of the major fault trends detected from the first-order vertical derivative map.

WEST						EAST				
N	N%	L	L%	L/N	Azimuth	L/N	L%	L	N%	N
13	12.7	25.4	11.0	2.0	0:<10	2.2	5.7	13.2	5.9	6
12	11.8	22.3	9.7	1.9	10:<20	2.5	9.7	22.5	8.8	9
7	6.9	12.4	5.4	1.8	20:<30	1.3	2.9	6.7	4.9	5
11	10.8	32.1	13.9	2.9	30:<40	1.6	5.7	13.2	7.8	8
13	12.7	37.1	16.1	2.9	40:<50	0.0	0.0	0.0	0.0	0
10	9.8	31.4	13.6	3.1	50:<60	1.5	1.3	3.0	2.0	2
2	2.0	3.5	1.5	1.7	60:<70	0.0	0.0	0.0	0.0	0
1	1.0	4.0	1.7	4.0	70:<80	1.4	1.2	2.7	2.0	2
1	1.0	1.3	0.6	1.3	80:≤90	0.0	0.0	0.0	0.0	0
70	68.6	169.4	73.4		S um		26.6	61.3	31.4	32

N=Number L=Length

Pre-Miocene (Figure 10(a)), and the L%; N% within 10° of arc from the north were summed in Table 2 and imaged as a rose diagram in Figure 11(a). The peaks in the azimuth classes indicate the dominance of the westerly oriented fault trends, which are characterised by a broad spectrum of distribution. The large peaks to the west indicate that the Clysmic (old GOS) is the principal controlling trend on the basement surface. The peaks from N5°W to N55°W are looked upon as possible variants/branches of the Clysmic/GOS trend that may be due to shifting of the northern compressive force to the west. Another effective trend can be seen oriented in the N10°-30°E (Aqaba trend), which is less abundant.

The stress diagram and strain ellipse (Figure 11(b)) were created to describe the stress forces and associated shear fractures acting on the region. Detected trends interpreted from the Bouguer aomalies were used in combination with the idea of possible reorientation of stress (Mckinstry 1953), resulting from variations in direction and intensity of the lithostatic pressure at depth to visualise the shear fractures and tectonics of the area. Analysis of the forces dynamics indicates that the Precambrian basement rocks were subjected to two different types of forces which largely controlled the structural setting of the area; the NNW to NW compressive force (I,II), which was active for a long period contemporaneous with the ENE to NE extensional force (III,IV). The primary fractures resulted from these two forces has formed in the northwest direction as a first-order major faults (F1, F2). Other primary fracture system (thrust/reverse faults) was formed in the NE direction at a right angle to the axis of the NW-compressional force. The counter-clockwise rotation of these tectonic forces led to produce other complementary sets of deformations (F3and F4). It is believed that the structural elements (F3, F4) that are belonging to the GOS (N45°W) and Aqaba (N15°E) trends, were produced lately as secondary shear fractures by conjugation of these two forces (Meshref 1990). Generally, the interaction between these two stress forces led to dividing the area into segments of different sizes, tilts, and depths. The tectonic model suggests that the earlier phase of opening of the GOS and the related stress forces to occur in the Precambrian age.

10. Gravity modelling

The inverse modelling technique was applied to the gravity data before and after the stripping process in order to confirm the shallower constituents and to deduce the deeper configurations. The first profile was taken in the E-W direction passing across five wells while the second modelled profile stretches in the NW-SE direction controlled by sex wells (Figure 7 and Figure 9(a)). The sedimentary cover was subdivided into four lithologic groups; the Post-Miocene, Middle-Miocene, Lower-Miocene, and Pre-Miocene rock units. These packages were designed as 2D layers controlled by the boreholes information and results of the seismic data interpretation. The bulk density of each lithostratigraphic unit was averagely assigned as

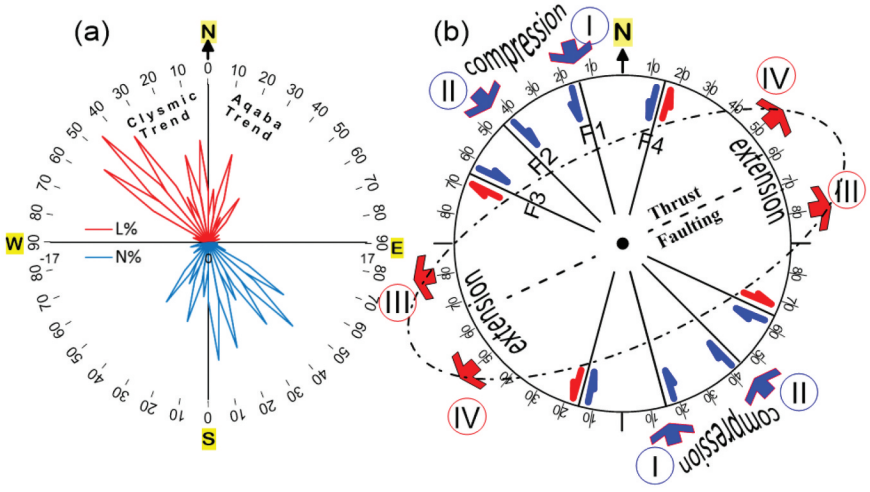

Figure 11. Statistical lineament analysis (a) rose diagram of the different structural trends and (b) stress-strain diagram of the study area, as was deduced from gravity-stripping map on top of Pre-Miocene.

driven from wells data. The basement was divided into blocks of different shapes, sizes, and depths, to reduce the misfit between the calculated and observed profiles. Every block was iteratively modified in terms of mass density and geometry to help in matching the gravity anomalies. The models were constructed using GM-sys software, included in the Oasis Montaj Package v. 8.3. 2014.

The first model (Figure 12(a)) was constructed before the gravity stripping, taken from the Bouguer anomaly map (Figure 7) along the profile (AA') in E-W direction. The characteristic feature of this model is the presence of a high gravity anomaly in the centre, between two gravity lows to the east and west. The gravity maximum was interpreted as an anticlinal structure or uplifted basement block (B2) that separates between two sedimentary basins to the east and west that vary greatly in lithology and depth. The eastern flank is characterised by a large in lithology, with a thick section of the Lower-Miocene (~2450 kg/m^3), Middle-Miocene (~2820 kg/m^3) and Post-Miocene (~2200 kg/m^3) sediments. The western flank contains a thicker section of the Pre-Miocene sediments (~2470 kg/m^3), with a noticeable thinning of the overlying strata. The depth to basement varies laterally with distance, where the depth to the uplifted blocks varies from 2.5 to 3 km while to the downfaulted ones ranges between 3.5 and 4.5 Km.

The 2D model in Figure 12(b) was constructed after the layer stripping process, along the same profile (AA') in E-W direction (Figure 9(a)). The upper part of the model shows two high gravity anomalies correlated with two basement uplifts (F2 and F6) in the lower portion. The model exhibits nearly the same geometry of the sedimentary layers, controlled by the well data and seismic reflection outputs. The density of the stripped layers was assigned to be zero because of their gravity effects have been removed from the observed gravity data. The density of the Pre-Miocene rocks was averagely assigned based on FDC of some boreholes. The shape and density of the basement blocks were iteratively fitted to obtain a good match between the calculated and observed anomalies.

In general, both of the two models show a good fit between the observed and calculated anomalies along with the gravity profiles. They exhibit nearly the same distribution and numbers of blocks with slight modification in the geometry, depth, and density. They reveal that the basement surface is uneven, consists of uplifted and downfaulted blocks, with a regional dip regime to the east. The structure was affected by a set of Clysmic faults which throw down to the east and west forming local grabens. These normal faults start on the basement surface, grow upwardly cutting across the Pre-Miocene sequence and die out into the Miocene section. The models indicate normal tilted fault blocks due to rifting, with no igneous intrusions penetrate the sedimentary sequence.

Second model (Figure 13(a)) was constructed along the profile BB' in the NNW-SSE (strike) direction on the Bouguer anomaly map (Figure 7). The profile cuts across a geologic high feature separates between two fill-sediment basins to the east and the west. The ambiguity inherent in the gravity data was reduced through a set of wells, which used as constraints for the sedimentary layers. The profile passes through six boreholes which largely control the thickness and depths of the different lithostratigraphic units. The observed profile in the upper section of the model shows a large gravity variation from the north to the south, which is closely associated with the basement relief. The high gravity anomalies are correlated with basement highs while the low gravity anomalies are corresponding to grabens. The basement surface seems to be well controlled by a set of cross-gulf faults of different throws and tilts. The relatively uniform thickness/depth of the Miocene layer suggests these transverse faults to be of small vertical displacement. The normal density values (2.630–2.680 g/cm^3) of the proposed polygons indicate that there are no magmatic flows along this transect, and suggest that the

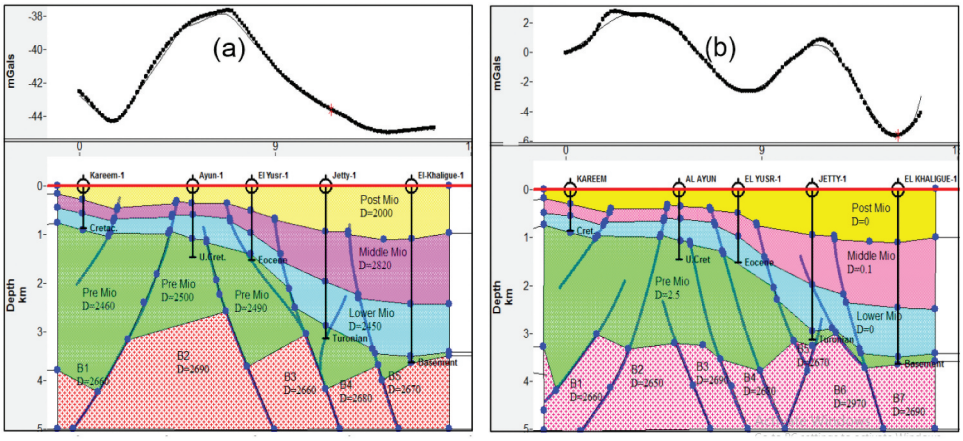

Figure 12. Gravity modelling along profile A-A' (a) before stripping, and (b) after tripping.

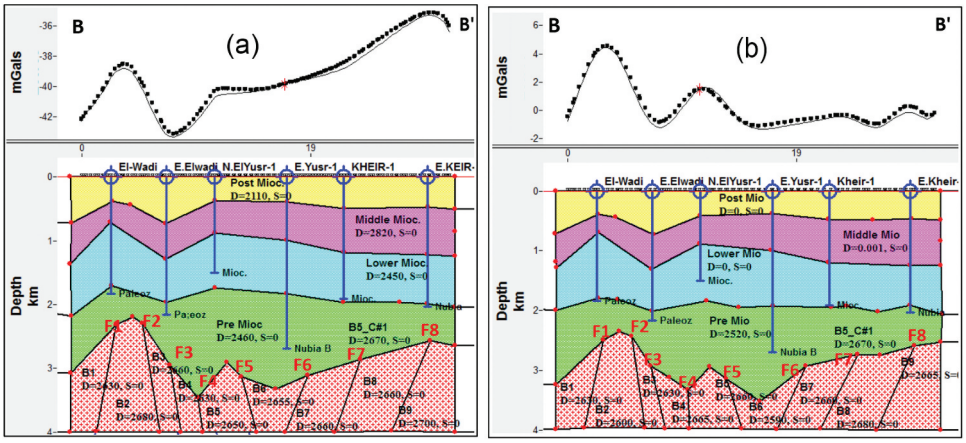

Figure 13. Gravity modelling along profile B-B′ (a) before stripping, and (b) after tripping.

gravity highs are primarily due to structural uplifts. The model reveals that the Pre-Miocene section was deposited on a rough basement surface, with great thickness variations from north to south. It generally presents a relatively thin sedimentary section along this transect, where the basement lies at depth ranges from 2 to 3.5 km.

The 2D model in Figure 13(b) was established after doing layer stripping (on top of Pre-Miocene), along the same profile BB' (Figure 9(a)). The modelled profile exhibits nearly the same geometry and distribution of Miocene–Post-Miocene strata, as controlled by wells and constrained by seismic mapping. The densities of the stripped layers were proposed to be zero while the density of the Pre-Miocene and basement rocks are iteratively inverted to reach the best fitness between the calculated and observed gravity profiles. Generally, the profile shows similar subsurface configurations that give the same structural conclusion obtained previously from Figure 13(a). It displays a comparable style of faults, tilt-blocks and alike distribution exist in Figure 13(a) with slight improvements on top of Pre-Miocene section and basement surface. The basement surface was deformed by a set of normal faults (F1-F8) of different tilts and throws, which could be correlated with those that occur in Figure 9. They confirm that the gravity signatures are closely linked with basement configurations where gravity minima are associated with troughs while gravity maxima are correlated with uplifts. The harmony between the gravity profile and basement relief indicates that the faulting is the source of structural complexity in the area.

Other two examples of density models were constructed along two different seismic lines in the strike and dip directions to confirm the shallower structures and to deduce the deeper source bodies. They focus attention on the upmost 4 km of the earth's crust; including the sedimentary section as well as the upmost portion of the basement rocks. The major sedimentary rock units were modelled as 2D layers, proposing a homogenous nature with average density for each formation as driven from density logs. The geometry of the sedimentary strata was adjusted based on seismic line interpretation. The third model (Figure 14) was constructed along the seismic line WM-41 (Figure 2) for a distance of about 11 km in the NW-SE (strike) direction. The seismic section was tied with two boreholes (Jetty-1 well and El-Khaligue-2) which considered as start points for controls. The undefined portion of the models was iteratively controlled until obtaining an acceptable fit between the calculated and observed anomalies. The interpreted structure indicates that the regional dip regime along this transect is to the west with a slight increase in the thickness of the sedimentary section. The model exhibits general thickening of the Miocene strata particularly Lower-Miocene Rudies Formation. The Miocene strata is dissected by a set of normal faults of different tilts and throws, forming horsts and grabens. The majority of these faults appear to originate from Pre-Miocene and die out in Upper-Miocene section. The Post-Miocene section thickens towards the centre with no divisible fractures deform the surface layer. The Pre-Miocene section seems to be thinner, with a noticeable northward increase.

The fourth model (Figure 15) was constructed in the E-W trend (dip direction) along seismic section WM-12 (Figure 2), passing through the coastal basin (El-Khaligue graben). The model shows a regional dip regime to the east with a gradual increase in the thickness of the sedimentary layers towards the gulf. The Miocene structure shows nearly a uniform distribution of Miocene layers, with a general slopping down to the east. The Miocene structure exhibits a few number of long faults (Clysmic faults) that seem to be start in Pre-Miocene and vanish in Upper-Miocene before reaching the surface. The normal density of the basement rocks (2670 kg/cm^3) may give indications support absence of any magmatic flows along cracks. Generally, the density models in the E-W and N-S directions allow understanding the

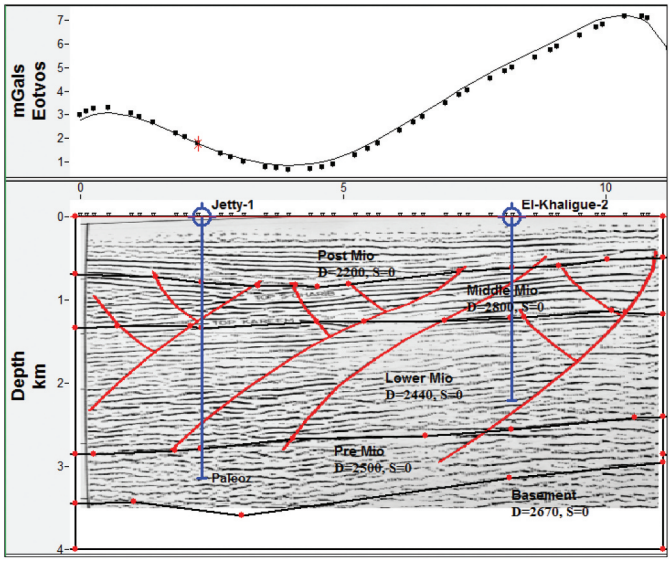

Figure 14. Gravity modelling along seismic section WM-41in the N-S (strike) direction.

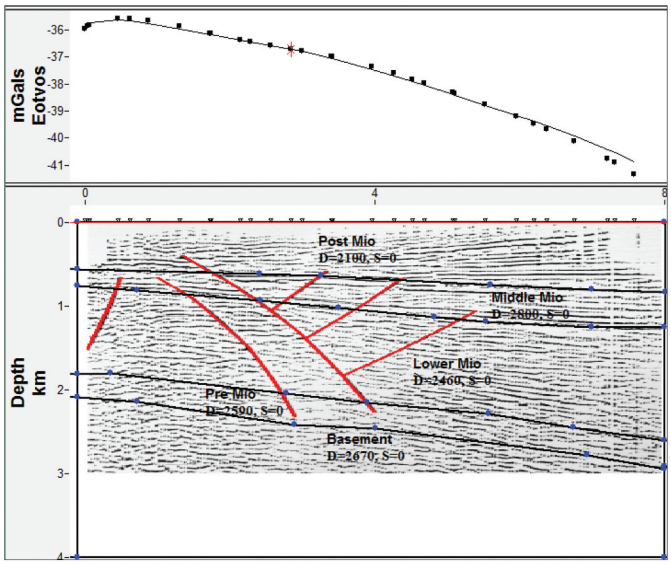

Figure 15. Gravity modelling along seismic section WM-12 in the W-E (dip) direction.

geometry and deep source structure, as well as identification of block-faults. Table 3 shows a comparison between densities of all rock units as driven from available well data and from stripped values.

The modelled profiles were compared with a stratigraphic cross section (Figure 16), which was taken in the dip direction (E-W), pass through a set of five wells. The cross-section exhibits two main basinal areas to the east and west, filled with different sediments. The Pre-Miocene sediments were excessively deposited in the western basin alongside Nubian Massif unconformably overlies the basement, whilst the Miocene basin has formed in the eastern side parallel to the GOS, unconformably overlies the Eocene ridge. The stratigraphic sequence in both of these two sub-basins is characterised by the presence of local and regional erosional unconformity surfaces as well as normal faults that complicate the structure. The surface layer seems to be not much deformed, where a thick layer of Pliocene-recent sediments unconformably overlain the Middle-Miocene rocks due to missing a part of the Upper-Miocene section.

Table 3. Average densities of major rock units as driven from available wells and from stripped values.

Rock Units	Densities from Wells (kg/m3)	Densities from stripped values (kg/m3)
Post-Miocene	1.810–2.340	~ 2.200
Upper-Miocene	1.920–2.120	~2.460
Middle-Miocene	2.590–2.910	~2.800
Lower-Miocene	2.310–2.540	~2.420
Pre-Miocene	2.410–2.650	~2.590
Basement	- - - -	~2.650–2.690

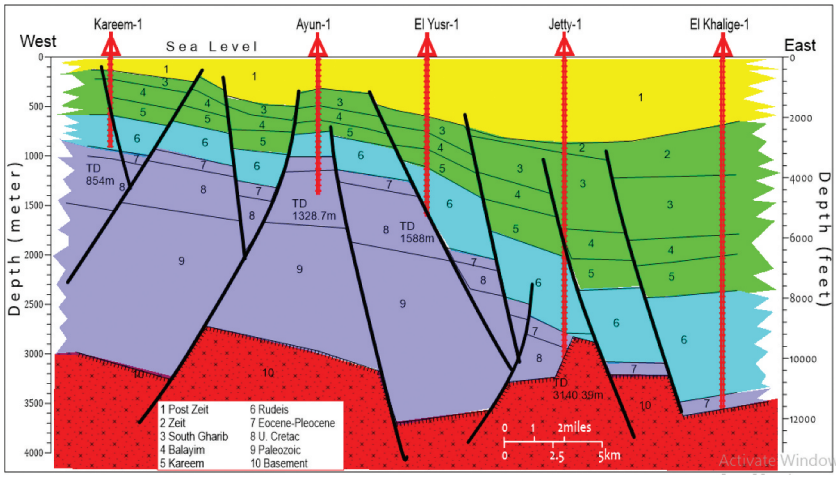

Figure 16. Stratigraphic cross section between five wells drilled in the study area in the E-W direction.

11. Discussion

Close inspection of the Bouguer anomaly map shows the dominance of the negative gravity values everywhere, which has been primarily interpreted to be due to a thick sedimentary cover. The gravity minima with low relief contours were interpreted to be correlated with sub-basins, while high gravity anomalies were essentially regarded to be the expression of structural uplifts.

The gravity anomalies are greatly influenced by the subsurface density heterogeneity, in particular, those exist in the Miocene strata. The percentage of the anhydrite-salt rocks is very changeable and lead to variations in the density of the formation. The density increases with the presence of anhydrite rocks of Ras Malaab evaporite group and/or the dense limestone of Gharandal group, while it noticeably decreases with an excessive thickness of the low-density halite of South Gharib and/or Rudeis sandstone. This nonlinear variation with depth extremely has a great impact on the gravity anomalies, consequently layer striping.

The stripping calculations assume the mean density of the surface layer (~2200 kg/m^3) is not largely variable either laterally or vertically, suggesting that the thickness of Pliocene-recent is of prime importance in calculating its gravity effect. As well, the Rudeis sands is characterised by a low range of density (~2450 kg/m^3), which may indicate that the thickness variation of Lower-Miocene section is very efficient in calculating its gravity effect. Contrary, the dense evaporite of Middle-Miocene rocks (~2800 kg/cm^3) is very effective in calculating their gravity effects.

The striping process is very effective in removing the undesired effect of shallower contaminations from the gravity data. The stripped map revealed gravity anomalies which do not exist before, which are of prime interest in deeper clarifications. The gravity maxima expect to be prospective uplifts and encourage drilling of these untested highs at the Pre-Miocene level.

The combination between the horizontal gradient filter and maximum curvature filter was useful to shed light on the deep geologic complexity beneath the Miocene evaporites from the stripped map. The linear forms surrounding the anomalous features from the east and west are referring to locations of the longitudinal faults (Clysmic trend). The continuity of these linear features is limited by the horizontal movement of the transverse faults of the NE-SW (Aqaba) trend. The intersection between these cross-faults has divided the area into blocks, and control many of oil traps.

The lineaments analysis detected two major tectonic trends; the NW to NNW trend which is the most prominent and more abundant, besides another less pronounced fault trend in the NNE to NE direction. These two old trends represent two principal fracture systems affected the basement and the overlying strata. The Clysmic trend is the most significant among all and plays the main role in complicating the structural setup of the area. The high percentages of length (L%) and the large number (N%) of these old trends may reflect the high intensity of their acting forces.

The tectonic model portrays possible stresses which affected the area and their relations with the crustal deformation and plates motion. The stress-strain diagram suggests two main stress forces of deformation that are closely related to the Tethyan plate tectonics. The old GOS (Clysmic) trend has primarily formed by the rift phases resulting from the opening of the Paleo-Tethys under the influence of NE-SW tensional forces (Meshref 1990), which was reactivated due to the Caledonian cycle of early to Mid-Palaeozoic (Said 1990). Lately, it was rejuvenated during Tertiary-Quaternary times due to active tensional movement of Arabia relative to Africa (Brown et al. 1989). The other effective tectonic trend is the Aqaba fault trend which has a left-lateral movement produced by the northeast movement of the Arabian plate relative to

Africa. El Gaby, 1987 attributed the Aqaba trend to the Precambrian time and developed in the Tertiary, dated as younger than the Gulf of Suez and Red Sea (Youssef 1968).

In comparison between the two models before and after the stripping, it is found that the stripped model (b) has a more powerful resolution in defining the deep geologic changes. Model (a) is characterised by one gravity high associated with basement uplift, while model (b) exhibits the presence of two maxima correlated with two uplifts. Such a Pre-Miocene high may be of geologic importance since it provides favourablea condition for oil accumulations from the surrounding sub-basins.

Presence of thick section of the Pre-Miocene deposits to the west, and the Miocene basin towards the east may suggest that the basement surface was at first sloping westwards where the Pre-Miocene sediments were accumulated alongside the Red Sea hills. Afterwards, during the Eocene, the area seems to be lifted up, and tilted regionally eastwards, where the Miocene sedimentary basin was formed along the western coast of the gulf.

The rapid changes in lithology and thickness of the formations may be considered as a good evidence for the active tectonics of the area during different geologic times. The sedimentary sequence shows, at first, a main depositional basin of the Pre-Miocene clastic rocks to the west, with a noticeable decrease in the thickness towards the east. Subsequently, with the beginning of the Middle Miocene age, a change in the lithology/location of sedimentation had taken place, where the Miocene evaporite sediments has been excessively deposited alongside the GOS coast. The Post-Miocene basin appears undeformed, which may indicate that the area is recently inactive. The differential load of deposition between the western basin and the eastern basin may suggest a kind of isostatic unbalance.

12. Conclusion

Detailed geophysical analysis of the gravity data after the stripping process have proven to be valuable in the deep exploration operation. By this way, it reached large depths (near basement) where the efficiency of the seismic reflection is very low down. The stripping process remove the gravity effect of the shallow contaminations, of the large significant influence, from the original data. After that, filtering of the stripped map has succeeded in finding out the hidden Pre-Miocene highs, in delineating the local basins within the major depression, and in revealing the deep fractures and associated basement structures. The structural inferences exhibit two main basinal areas of different characteristics; the Miocene basin (El-Khaligue basin) to the east, alongside the GOS, and the Pre-Miocene basins to the west (W. Kareem, S. El-Yusr, W. Kheir) beside the Nubian Massif. They were separated from each other by a longitudinal ridge-like structure that extends in the NNW-SSE direction from El-Wadi-El Yusr to Kheir. The study indicates that the basement surface is formed from tilted-blocks separated by normal faults of different throws and tilts. The depth to the downfaulted basement blocks varies between 3.5 and 4.5 km while for the uplifted ones is from 2.5 to 3 Km, the matter that has been confirmed by SPI map. The models provide no evidence of any dense materials of mantle penetrate the basement surface. The study indicates that faults are the major structural elements and play the main role in complicating the area. The westerly-trending faults (Clysmic trend) are the most dominant and more abundant than others, and were obliquely cut or offset by a set of easterly oriented faults (Aqaba trend). These cross-faults thought to be a Pre-rift structural fabric since they heavily exist on the basement surface. The basement faults have continuously rejuvenated upwardly into the Pre-Miocene rocks, and vanished within the Miocene strata before reaching the surface. The work indicate that the area has the same structural-tectonic conditions of the tural-tectonic condition productive oil fields. The matter which may encourage further deep exploration operations, especially the untested gravity maxima which are correlated with the basement uplifts.

Disclosure statement

No potential conflict of interest was reported by the authors.

ORCID

Ahmad Azab http://orcid.org/0000-0002-8652-1610
Shokry Soliman http://orcid.org/0000-0003-0489-5801

References

Abu El-Ata ASA, Helal A, 1985. Gravity stripping as a tool for deducing the paleotectonic implications for the western coast of the GOS, Egypt. Proc. 4th Ann. Meet EGS. Cairo, Egypt.

Abu El-Ata ASA, Helal A, 1986. Role of gravity stripping in subsurface modeling of the western coast of the GOS, Egypt, Bull. Faculty of science Aswan University

Affleck L. 1963. Magnetic anomaly trend and spacing patterns. Geophys. 28:379–395.

Alasonati TS, Arov AZ, Bielik M, Otze J. 2008. Stripped image of the gravity field of the carpathian-pannonian region based on the combined interpretation of the celebration 2000 data. Geol Carpathica. 59:199–209.

Alsharhan AS. 2003. Petroleum geology and potential hydrocarbon plays in the Gulf of Suez rift basin, Egypt. Am Assoc Petrol Geol Bull. 87:143–180.

Azab AA, Ramadan MA, El-Sawy MZ. 2018. An integrated analysis of gravity and well data for deep-seated structural

interpretation: a case study from ras budran oil field Gulf of Suez Egypt. J Pet Explor Prod Techn. http://doiorg/101007/s13202–018–0514–8.
Bible K, John L, 1961. Old gravity never die world petroleum. 48–66
Bielik M, 1988. A preliminary stripped gravity map of the pannonian basin physics earth planet 51:185–189
Bielik M, Rybakov M, Lazar M, 2013. Estimation of reliability and accuracy of geological gravity back stripping the leading edge. 32:410–416
Bayoumi AJ. 1983. Tectonic origin of Gulf of Suez Egypt as deduced from gravity data. In: Geyer RA, Moore JR, editors. Handbook of geophysical exploration at sea reference, CRC press. Cairo:417–432.
Bosworth W, McClay K. 2001. Structural and stratigraphic evolution of the Gulf of Suez rift, Egypt: a synthesis. In: Ziegler PA, Cavazza W, Robertson AHF, CrasquinSoleau S, editors. Peri–tethys memoir 6: peri–tethyan rift/wrench basins and passive margins, Vol. 186. Mémoires du Muséum National d'Histoire Naturelle de Paris, Paris, France: 567-606.
Bosworth W, Durocher S. 2017. Present–day stress fields of the Gulf of Suez, Egypt: based on exploratory well data Non–uniform regional extension and its relation to inherited structures and local plate motion. J Afr Earth Sci. 136:136–147.
Bosworth W, Khalil S, Clare A, Comisky J, Abdelal H, Reed T, Kokkoros G. 2014. Integration of outcrop and subsurface data during the development of a naturally fractured Eocene carbonate reservoir at the east Ras Budran concession, Gulf of Suez, Egypt. In: Spence GH, Redfern J, Aguilera R, Bevan TG, Cosgrove JW, Couples GD, Daniel JM, editors. Advances in the study of fractured reservoirs, Geological Society; London, Special Publications 374:333–359.
Bosworth W, Taviani M, Rasul N, 2016. Neotectonics of the red sea, Gulf of Suez and Gulf of Aqaba In: Workshop on the Geological Setting Oceanography and Environment of the Red Sea. 31–34 Saudi Geological Survey. 14–17 February Jeddah, Proceedings
Brown GF, Schmidt DC, Huffman C. 1989. Geology of the Arabian peninsula shield area of western Saudi Arabia. US Geol Sur Prof Pap, 560:188.
EGPC (Egyptian General Petroleum Corporation). 1986. *Geological Map of Egypt Scale 1:500000*, Conoco Coral, Palestine Rd, Maadi. Cairo, Egypt
Garfunkel Z, Bartov Y. 1977. The tectonics of the suez rift. Geol Surv Isr Bull, 71:44p.
Gupta S, Underhill JR, Sharp IR, Gawthorpe RL. 1999. Role of fault interactions in controlling syn–rift sediment dispersal patterns, miocene, abu alaqa group, suez rift, sinai, Egypt. Basin Res. 11:167–189.
Hammer S. 1963. Deep gravity interpretation by stripping. Geophys. 28:369–378.
Henderson RG, Zeitz L. 1949. The computation of second vertical derivative of geomagnetic fields. Geophys. 14:517–534.
Hewaidy AA, Mandur MM, Farouk S, El-Agroudy IS. 2016. Integrated planktonic stratigraphy and paleo environments of the lower–middle-miocene successions in the central and southern parts of the Gulf of Suez, Egypt. Arab J Geosci. 9:1–32. http://dxdoiorg/101007/s12517–015–2108–9).
Jackson CAL. 2008. Sedimentology and significance of an early syn–rift paleovalley, wadi tayiba, suez rift, Egypt. J Afr Earth Sci. 52:62–68. http://dxdoiorg/101016/jjafrearsci200803007).
Khalil SM, McClay KR. 2008. Structural control on syn–rift sedimentation, northwest red sea margin, Egypt. Mari Pet Geol. 26:1018–1034.
Krajňák M, Bielik M, Makarenko I, Legostaeva O, Starostenko VI, Bošanský M. 2012. The stripped gravity map of the turčianska kotlina basin. Cont Geophys Geodesy. 42:181–199.
McClay KR, Nicols GJ, Khalil SM, Darwish M, Bosworth W. 1998. Extensional tectonics and sedimentation, eastern Gulf of Suez, Egypt. In: Purser BH, Bosence DWJ, editors. Sedimentation and tectonics of rift basins: red sea–Gulf of Aden. London: Chapman and Hall; p. 223–238.
Mckinstry HE. 1953. Shears of the second order. Am J Sci. 251:401-414.
Meshref WM. 1990. Tectonic framework of Egypt. In: Said R, editor. The geology of Egypt (Vol. 19). Rotterdame (Brookfeild): A.A. Blkema; p. 1013–1026.
Montenat C, Jarrige OJ, Richert JP. 1998. Rift development in the Gulf of Suez and the northwestern red sea: structural aspects and related sedimentary processes. In: Purser BH, Bosence DWJ, editors. Sedimentation and tectonics of rift basins: red sea–Gulf of Aden. Chapman and Hall: London; p. 97–116.
Morley CK. 1995. Developments in the structural geology of rifts over the last decade and their impact on hydrocarbon exploration. In: Lambiase JJ, editor. Hydrocarbon habitat in rift basins (Vol. 80). Geol. Soc. London: Special Publ; p. 1–32.
Moustafa AR. 1976. Block-faulting in the Gulf of Suez DEMINEX EGYPT, 5th, Explor. Semin. of EGPC, Cairo:36p.
Moustafa AR. 1993. Structural characteristics and tectonic evolution of the east–margin blocks of the suez rift. Tectonophysics. 223:381–399.
Nabighian MN. 1972. The analytic signal of two-dimensional magnetic bodies with polygonal cross-section: its properties and use for automated anomaly interpretation. Geophys. 37(3):507–517.
Nabighian MN, Grauch VJS, Hansen RO, LaFehr TR, Li Y, Peirce JW, Philips JD, Ruder ME. 2005. The historical development of the magnetic method in exploration. Geophys. 70:33–61.
Oasis Montage v 8.3., H.j., 2014. Oasis montaj mapping and processing system. Geosoft Inc. Toronto Ontario Canada, http://www.geosoft.com
Otsuka T, Ogawa K 1977. Combined seismic and gravity interpretation in west bakr area, Gulf of Suez, Egypt. Report of Technology Research center, JPC (Tokyo): 6
Patton TL, Moustafa AR, Nelson RA, Abdine SA. 1994. Tectonic evolution and structural setting of the suez rift. In: Interior Rift basins, (Ed. Landon, s.), AAPG Memoir, London, 59:9–55.
Pietrantonio G, Devoti R, Mahmoud S, Riguzzi F. 2016. Kinematics of the suez–sinai area from combined GPS velocity field. J Geodyn. 102:231–238.
Reeves CV, 2005. Aeromagnetic surveys, principles, practice and interpretation. Geosoft. 155
Reid AB, Allsop JM, Granser H, Millett J, Somerton IW., 1990. Magnetic interpretation in three dimensions using euler deconvolution geophysics. 55:80–91
Roberts A. 2001. Curvature attributes and their application to 3D interpreted horizons. Eur Assoc Geoscientists Eng. 19:85–100.
Roest WR, Verhoef J, Pilkington A. 1992. Magnetic interpretation using the 3D analytic signal. Geophys. 57:116–125.
Rohais S, Barrois A, Colletta B, Moretti I. 2016. Pre–salt to salt stratigraphic architecture in a rift basin: insights from a basin–scale study of the Gulf of Suez. Egypt Arab

J Geosci. 9:317. http://dxdoiorg/101007/s12517–016–2327–8).
Rybakov M, Goldshmidt V, Fleischer L, Rotstein Y. 1998. Geological "stripping" of the gravity field of Israel. Isr J Earth Sci. 47:69–74.
Said R. 1990. The geology of Egypt. Rotterdam Netherlands: Balkema Publ; p. 734.
Schlumberger. 1984. Well evaluation conference, services Techniques, Schlumberger, France: 19–31.
Segev A, Avni Y, Shahar J, Wald R. 2017. Late oligocene and miocene different seaways to the red sea–Gulf of Suez rift and the Gulf of Aqaba–dead sea basins. Earth Sci Rev. 171:196–219.
Sharp IR, Gawthorpe RL, Underhill JR, Gupta S. 2000. Fault propagation folding in extensional settings: examples of structural style and syn–rift sedimentary response from the Suez Rift, Egypt. Geol Soc Am Bull. 112:1877–1899.
Sharp IR, Gawthorpe RL, Underhill Winn RD, Crevello PD, Bosworth W. 2001. Lower-miocene nukhul formation, Gebel el Zeit, Egypt: model for structural control on early synrift strata and reservoirs, gulf of suez. Am Assoc Pet Geol Bull. 85:1871–1890.
Simeoni O, Brueckl E, 2009. Gravity stripping supports tectonic interpretation of the eastern Alps. EGU General Assembly Geophysical Research Abstracts. 11:7355
Temraz M, Dypvik H. 2018. The lower-miocene nukhul formation, Gulf of Suez, Egypt: microfacies and reservoir characteristic S.J. Pet Explor Prod Techn. 8:85–98. https://doiorg/101007/s13202–017–0386–3.
Tenzer R, Hamayun K, Vajda P. 2009. Global maps of the crust 20 crustal components stripped gravity disturbances. J Geophys Res. 114:B05408.
Thompson DT. 1982. EULDPH–A new technique for making computer-assisted depth estimates from magnetic data. Geophys. 47:31–37.
Vajda P, Ellmann A, Meurers B, Vaníček P, Novák P, Tenzer R. 2008. Global ellipsoid–referenced topographic, bathymetric and stripping corrections to gravity disturbance. Stud Geophys Et Geodaetica. 52:19–34.
Young MJ, Gawthorpe RL, Sharp IR. 2002. Architecture and evolution of syn–rift clastic depositional systems towards the tip of a major fault segment, Suez Rift, Egypt. Basin Res. 14:1–23.
Youssef MI. 1968. Structural pattern of Egypt and its interrelation. Am Assoc Pet Geol Bull. 52(4):601–614.